Molecular dynamics simulations of pure methane and carbon dioxide hydrates: lattice constants and derivative properties

Joseph Costandy, Vasileios K. Michalis, Ioannis N. Tsimpanogiannis, Athanassios K. Stubos & Ioannis G. Economou

    View supplementary material ⎘

    Published online: 25 Oct 2016.

    Submit your article to this journal ⎘

    Article views: 20

    View related articles ⎘

    View Crossmark data ⎘

Taylor & Francis
Taylor & Francis Group

THERMODYNAMICS 2015

Molecular dynamics simulations of pure methane and carbon dioxide hydrates: lattice constants and derivative properties

Joseph Costandy [a,*], Vasileios K. Michalis [a], Ioannis N. Tsimpanogiannis [a,b], Athanassios K. Stubos [b] and Ioannis G. Economou [a]

[a]Chemical Engineering Program, Texas A&M University at Qatar, Doha, Qatar; [b]Environmental Research Laboratory, National Center for Scientific Research (NCSR) "Demokritos", Athens, Greece

ABSTRACT

We report extensive molecular dynamics simulation results of pure methane and carbon dioxide hydrates at pressure and temperature conditions that are of interest to various practical applications. We focus on the calculation of the lattice constants of the two pure hydrates and their dependence on pressure and temperature. The calculated lattice constants are correlated using second order polynomials which are functions of either temperature or pressure. Finally, the obtained correlations are used in order to calculate two derivative properties, namely the isothermal compressibility and the isobaric thermal expansion coefficient. The current simulation results are also compared against reported experimental measurements and other simulation studies and good agreement is found for the case of isothermal compressibility. On the other hand, for the case of isobaric thermal expansion coefficient good agreement is found only with other simulation studies, while the simulation studies are in disagreement with experiments, particularly at low temperatures.
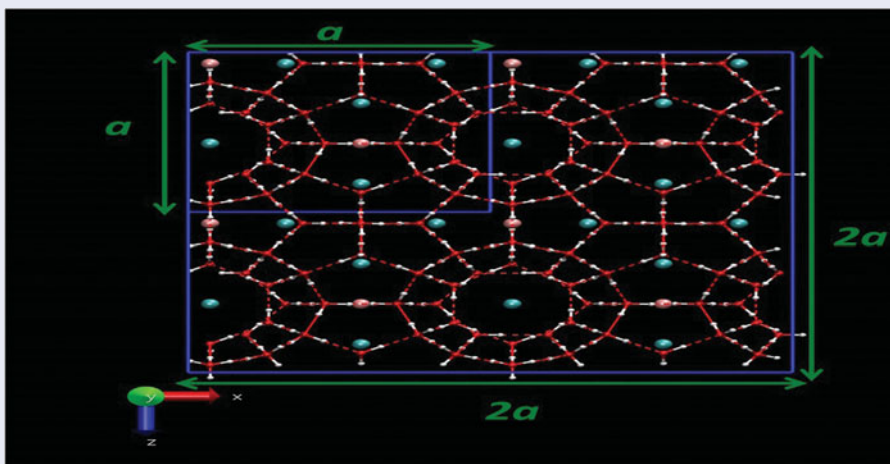
1. Introduction

The ability of clathrate hydrates to selectively incorporate significant amounts of guest molecules inside the three-dimensional cages formed by hydrogen-bonding water molecules could be utilised in a number of industrial applications [1,2]. In particular, of major interest are the storage and transportation of 'energy-carrier' (e.g. methane [3,4], hydrogen [5–7]) or environmentally related (e.g. carbon dioxide [8]) gases, and the separation of gas mixtures [9–11]. In all cases the structural properties of clathrate hydrates play an important role. For example, different cage sizes can result in different degrees of cage-filling, which subsequently results in different total amount of gas stored inside the hydrate structure (i.e. storage capacities). Similarly, change of the structural properties of clathrate hydrates can have a significant effect on the selectivity of gas mixture separations.

Experimental studies of measuring the hydrate lattice constants have indicated that the size of the hydrate unit cell, therefore the cage sizes as well, depends both on pressure and temperature [12–21]. Furthermore, experimental measurements have shown that guests of different sizes that form a particular hydrate structure can result in different values for the lattice constant of the particular hydrate structure [22–24]. Accurate knowledge of the structural properties of hydrates, therefore, is of critical importance for either the design of novel processes or for the thermodynamic description and optimisation of currently existing ones. Molecular dynamics (MD) simulations can provide an alternative approach in calculating structural properties of clathrate hydrates [25]. Such computational studies [26–31] have reached to conclusions that are similar to those obtained by the experimental observations.

In recent MD studies, the phase coexistence envelope in the presence of hydrates for the case of pure methane [32–34] and carbon dioxide [35,36] hydrates have been calculated. To this purpose, the phase coexistence approach [37] was successfully utilised. It was established for the two particular cases of guests that in order to calculate accurately the hydrate equilibrium pressures, the following two requirements should be met: (1) the water model should predict accurately the melting point of ice, and (2) the combination of the water and guest molecule models should be able to give accurate guest solubilities in the aqueous phase. In these calculations, the TIP4P/Ice [38] and the TIP4P/2005 [39] water models were used. Also, recent Monte Carlo (MC) simulation studies [40–42] have used the TIP4P/Ice water model in order to calculate the methane storage capacities.

The current study is motivated by the need to examine the accuracy of the calculated lattice constants (i.e. defined as the length of the edge of the cubic hydrate unit cell) of pure methane and carbon dioxide hydrates at pressure and temperature conditions, as well as water/guest model-combinations, that are relevant to the aforementioned studies. Therefore, there is no effort here to identify the optimum combination of water and guest models that gives accurate lattice constant calculations with respect to experiments. A detailed study examining the issue has been reported recently by Ning *et al.* [43].

The manuscript is organised as follows. At first, we present the methodology used for the MD calculations performed. Next, we present initial comparisons with experimental measurements, followed by the MD results at the pressure and temperature conditions of interest. Subsequently, we utilise the MD simulations to calculate the isothermal compressibility, κ_T, and the isobaric thermal expansion coefficient, α_P. The calculated properties are compared against experimental measurements when available. The isothermal compressibility is an important parameter that is encountered during the interpretation of seismic data obtained during the geophysical surveys that are performed in order to identify natural hydrate deposits within off-shore oceanic sediments or on-shore permafrost settings. Finally, we end with the conclusions.

2. Methodology

Experimental studies for both the methane [44] and carbon dioxide [45] hydrates indicate that they adopt the cubic sI hydrate structure (space group *Pm3n*) for the pressure ranges that are relevant to the current study (i.e. up to 100 MPa for methane and up to 500 MPa for carbon dioxide). The actual values for pressure where hydrate structural transitions occur can be found in the relevant experimental studies [44,45]. A unit cell of the cubic sI hydrate structure consists of eight cavities that are formed by a three-dimensional network of 46 hydrogen-bonded water molecules, within which the methane or carbon dioxide guest molecules reside. In particular, it consists of two 5^{12} cavities and six $5^{12}6^2$ cavities. Figure 1(a) depicts a characteristic schematic of a single sI cubic hydrate unit cell where the lattice constant is clearly depicted.

In order to conduct the MD simulations, a solid slab of a $2 \times 2 \times 2$ sI hydrate supercell was initially prepared (see also the schematic of Figure 1(b)). The positions of the oxygen molecules within the unit cell were obtained from McMullan *et al.* [46]. The hydrogen atoms were attached to each oxygen atom in a random orientation, while respecting the geometry dictated by the chosen water force field. A single guest molecule (methane or carbon dioxide) was then placed at the centre of each cage, corresponding to the case of 100% cage occupancy. Cage occupancy is kept fixed throughout the simulations and does not vary with pressure or temperature. The unit cell was then duplicated in the *x*, *y* and *z* dimensions giving the supercell, which consisted of 368 water molecules and 64 guest molecules. Finally, a steepest descent energy minimisation was applied to find the positions of the hydrogen atoms, while fixing the oxygen atoms in order to avoid molecular overlap. This approach is an alternative to the commonly reported dipole moment minimisation [47], and also results in a structure that respects the Bernal and Fowler rules [48].

The water molecules were represented using the well-known TIP4P [49] molecular geometry. The two chosen force fields for this study were the TIP4P/Ice [38] and TIP4P/2005 [39], which are both rigid, non-polarisable models, where a Lennard-Jones interaction site is placed at the position of the oxygen atom, while positive charges
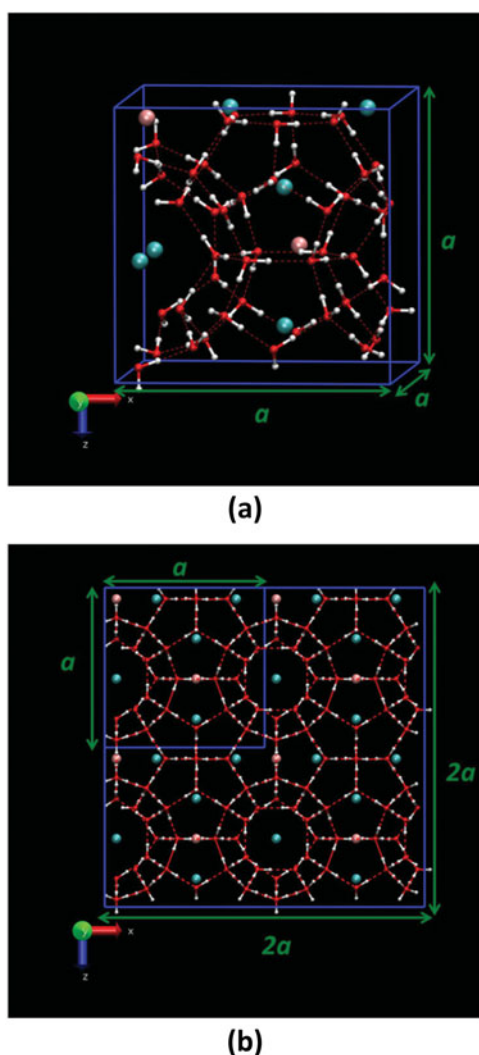
(a)

(b)

Figure 1. Schematic depicting the characteristic length (green arrows) that is equal to the lattice constant of sI hydrates: **(a)** a single sI cubic hydrate unit cell and **(b)** the two-dimensional projection of a 2 × 2 × 2 sI hydrate supercell. Notation used: red spheres denote oxygen atoms, white spheres denote hydrogen atoms, blue spheres denote the centre of the $5^{12}6^2$ cavities and pink spheres denote the centres of the 5^{12} cavities. The coordinates reported in Ref. [47] are used with the VMD tool for the visualisation. (For interpretation of the references to colour in this figure legend, the reader is referred to the web version of the article).

Table 1. Potential parameters of the TIP4P/Ice (water) [38], TIP4P/2005 (water) [39], OPLS-UA (methane) [50] and TraPPE (carbon dioxide) [51] models. The Lennard-Jones parameters are denoted as σ (size parameter) and ε/k_B (energy parameter), with k_B the Boltzmann constant. The charge is denoted as q. The distance, in Å, between atoms A and B is denoted as d_{AB}. The angle, in degrees, formed at a central atom B separating two A atoms is denoted as $\angle$A–B–A.

Force field	Atom	σ (Å)	ε/k_B (K)	q (e)	Geometry	
TIP4P/Ice (water)	O	3.1668	106.1	0.0	d_{OH} (Å)	0.9572
	H	0.0	0.0	0.5897	$\angle$H–O–H	104.5
	M	0.0	0.0	− 1.1794	d_{OM} (Å)	0.1577
TIP4P/2005 (water)	O	3.1589	93.2	0.0	d_{OH} (Å)	0.9572
	H	0.0	0.0	0.5564	$\angle$H–O–H	104.52
	M	0.0	0.0	− 1.1128	d_{OM} (Å)	0.1546
OPLS-UA (methane)	–	3.73	148.0	–	–	–
TraPPE (carbon dioxide)	C	2.800	27.0	0.700	d_{CO} (Å)	1.16
	O	3.050	79.0	− 0.350	$\angle$O–C–O	180

In the current study, the cross-interaction parameters between methane and water were calculated using the standard Lorentz-Berthelot (LB) combining rules [52]. For carbon dioxide–water, the cross-interaction distance parameters were calculated using the standard LB combining rule, while a modification (χ) was applied to the LB cross-interaction energy parameter between the oxygen of the carbon dioxide and the oxygen of water (all other cross-interaction energy parameters were calculated with the LB combining rules), that has values of 1.08 and 1.115 for TIP4P/Ice and TIP4P/2005, respectively, as calculated by Costandy *et al.* [36]. Furthermore, several tests were conducted using the standard LB combining rules to determine the effect, if any, of the modification of the combining rules on the lattice constant predictions.

All simulations were run in the isothermal–isobaric (NPT) ensemble using the GROMACS MD simulation package (version 4.6.5) [53–55]. The pressure and temperature coupling were implemented using the Berendsen scheme [56] with time constants of 0.5 ps. The pressure coupling used was anisotropic with the same compressibility in all three dimensions, such that each side of the simulation box can fluctuate independently. The leap-frog integrator scheme was used with a time step of 2 fs. The long range Coulombic interactions were handled with the particle mesh Ewald (PME) method [57]. The Lennard-Jones interactions were calculated with a cut-off distance of 11 Å.

The dependency of the lattice constants on pressure or temperature was obtained by conducting temperature scans at all pressures of interest to the study, or by conducting pressure scans at all temperatures of interest,

are positioned on the hydrogen atoms. The negative charge is placed on a virtual site M which lies along the bisector of the H–O–H angle. The two force fields differ in the values of the Lennard-Jones parameters, the position of M, and the magnitude of the charges. Methane was modelled using the OPLS-UA [50] force field parameters, which represents the methane molecule as a single, neutral Lennard-Jones sphere. Carbon dioxide was modelled using the rigid, non-polarisable TraPPE [51] force field, which represents the molecule as a linear chain of three partially charged Lennard-Jones sites. Parameters for these force fields are presented in Table 1.

respectively. In order to avoid starting from a frozen system that requires a long equilibration time, the initial velocities were generated at the highest temperature of interest at the particular pressure. However, if the highest temperature was below 280 K, the velocity was generated at 280 K. After an equilibration period of 1 ns, the system was cooled at a rate of 1 K per 20 ps until it reached the highest temperature of interest. The system was allowed a further 0.5 ns of equilibration, then a 5 ns period for calculation of the average lattice constant. The calculation was performed every 5 ps in this period, generating 1000 measurements, from which the average lattice constant was obtained. This procedure was repeated until the lowest temperature of interest at the given pressure was reached.

3. Results and discussion

3.1. Pressure and temperature correlation of the MD data

Of particular interest is the study of the lattice constants as a function of pressure (at constant temperature) or as a function of temperature (at constant pressure). Both cases are considered in the current study for pure methane and carbon dioxide hydrates. The MD-calculated lattice constants were fitted with second order polynomials for isothermal and isobaric scans of pressure and temperature, respectively, as follows:

$$a(P) = n_{P0} + n_{P1} \cdot (P/\text{bar}) + n_{P2} \cdot (P/\text{bar})^2,$$
$$\text{for } T \text{ constant} \qquad (1)$$

where P is in bar, n_{P0}, n_{P1} and n_{P2} are constants given in Tables SI-1 and SI-2 of the Supplemental Information for methane and carbon dioxide hydrates, respectively, and

$$a(T) = n_{T0} + n_{T1} \cdot (T/K) + n_{T2} \cdot (T/K)^2,$$
$$\text{for } P \text{ constant} \qquad (2)$$

where T is in K, n_{T0}, n_{T1} and n_{T2} are constants given in Tables SI-3 and SI-4 of the Supplemental Information for methane and carbon dioxide hydrates, respectively.

3.2. Comparison with experiments

Initially, we perform a series of comparisons with available experimental measurements and other reported MD studies for the cases of pure methane and carbon dioxide hydrates. Figure 2 shows the dependence of the MD-calculated methane hydrate lattice constants on pressure at 271.15 K using the TIP4P/Ice and TIP4P/2005 water force fields. The MD simulations are compared against the experimental measurements for the lattice

constants at 271.15 K and pressures in the range 50–1000 bar that were reported by Klapproth *et al.* [12] and obtained from crystallographic structure (i.e. Rietveld-type) full pattern profile refinements. Klapproth *et al.* [12] performed a series of neutron and hard-X-ray synchrotron diffraction experiments. We observe that the fits provide an excellent description of the MD simulations. Furthermore, the use of TIP4P/2005 water force field results in better agreement of the MD simulations with the experimental data when compared with the case of TIP4P/Ice. In particular, the percentage absolute deviation (% AD) of the lattice constant, a, defined as: %AD $= 100 \times |\frac{a^{\text{exp}} - a^{\text{MD}}}{a^{\text{exp}}}|$, where superscript 'exp' denotes experimental values and superscript 'MD' denotes the MD simulations, is in the range 0.11%–0.15% for the TIP4P/2005, while it is in the range 0.44%–0.52% for the TIP4P/Ice.

Figure 3 shows the dependence of the MD-calculated methane hydrate lattice constants on temperature at 1 bar. We observe that the second order polynomial fits provide an excellent description of the MD simulation data. We compare the MD simulations against the experimental data for the methane hydrate lattice constants reported by Ogienko *et al.* [16] and Shpakov *et al.* [13]. Shown in the figure are also the experimental data for the deuterated methane hydrate by Gutt *et al.* [14]. In addition, MD data reported by Jiang *et al.* [29], using the AMOEBA [59] and COS/G2 [60] polarisable water force fields, and the MD data reported by Jiang and Jordan [30], using the SPC/E force field, are shown as well. The use of TIP4P/2005 water force field results in better agreement of the MD simulations with the experimental data, particularly for temperatures above 150 K. The issue of temperatures lower than 150 K will be discussed further, later in this section. The results for the TIP4P/Ice of the current study and those by the AMOEBA [59] force field that were reported by Jiang *et al.* [29] are in very good agreement with each other.

The dependence of the MD-calculated methane hydrate lattice constant on temperature at 30 bar is shown in Figure SI-1 of the Supplemental Information. Comparison is made between the MD simulations of the current study, using the TIP4P/2005 water model, the MD simulations reported by Docherty *et al.* [28], using the TIP4P/2005 water model, and the experimental data for the methane hydrate lattice constants that were reported by Sun and Duan [61] at 30 bar. Excellent agreement is found between the two simulation studies. Both MD simulations underestimate the experimental data by 0.10%–0.20% (% AD).

The dependence of the calculated carbon dioxide hydrate lattice constants on temperature at 1 bar is shown in Figure 4. Two cases of the modification parameters χ are examined for each one of the TIP4P/Ice and
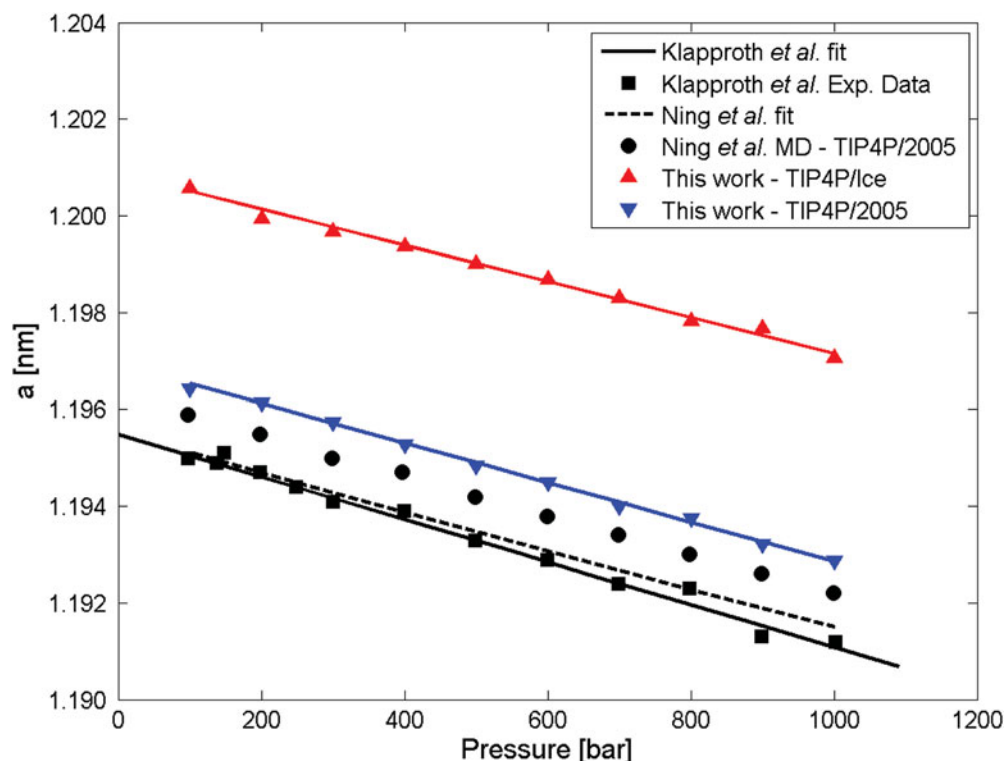
Figure 2. MD results for methane hydrate lattice constants as a function of pressure at 271.15 K using the TIP4P/Ice (red up triangles) and TIP4P/2005 (blue down triangles) force fields for water. The red and blue solid lines are linear fits of the MD data for the TIP4P/Ice and TIP4P/2005 force fields, respectively. The black solid line depicts a fit to the experimentally determined lattice constants (black squares) at 271.15 K and pressure range by Klapproth et al. [12]. The black circles denote the MD results by Ning et al. [43] using the TIP4P/2005 and OPLS-UA for water and methane, respectively, while the black dashed line denotes the fit of the MD data using the TIP4P/2005 and TKM-AA [58] models, respectively. (For interpretation of the references to colour in this figure legend, the reader is referred to the web version of the article).

TIP4P/2005 water models. A value of $\chi = 1$ corresponds to the case of calculating the cross-interactions using the LB combining rules. The remaining cases correspond to calculating the cross-interactions using modified LB combining rules that give accurate predictions for the carbon dioxide solubilities in the aqueous phase. By changing the modification parameter, χ, we observe a minimal effect on the calculated values of the hydrate lattice constants. The MD simulations are compared against the experimental data by Ikeda et al. [17] and Udachin et al. [19]. For temperatures above 100 K the use of TIP4P/Ice results in better agreement between the MD simulations and the experimental measurements. Shown also in Figure 4 are the MD results by Ning et al. [43] using TIP4P/2005 force field for water and TraPPE for carbon dioxide, which are in excellent agreement with the current simulations. Shown also are the MD simulations by Jiang and Jordan [30] using the SPC/E force field for water, while using the Zhang-Duan force field for carbon dioxide [62,63].

A general observation, obtained from a number of classical MD simulation studies [29,30,43], is that the lattice constants have an almost linear dependency on temperature (at 1 bar), even for very low temperatures (i.e. less than 150 K). On the other hand, a noticeable change of the slope is observed for the reported experimental measurements of lattice constants [13,16,19,20], for temperatures that are lower than approximately 150 K. A detailed discussion of the issue of correcting this behaviour through the use of path integral Monte Carlo simulations is provided by Vega and co-workers [64,65]. Also in a recent study, Constandy et al. [66] presented a correction for the classical MD simulations that results in obtaining lattice constants that exhibit the correct dependency on temperature. Therefore, the issue is not examined any further in the current study. The particular study [66] also examined the effect of partial cage occupancy.

3.3. MD calculations

Subsequently, we examine the dependence of the hydrate lattice constants on pressure and for various temperatures using the TIP4P/Ice and TIP4P/2005 water force fields. In particular, for the case of methane hydrate we performed calculations at 200, 250 and 300 K and pressures up to
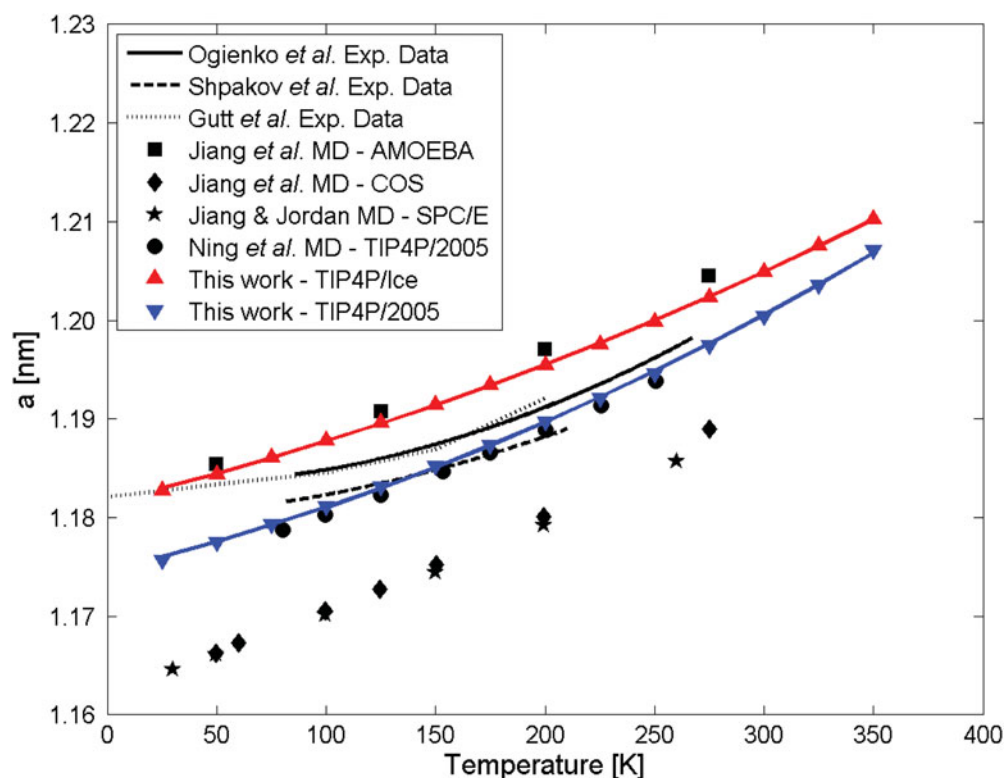
Figure 3. MD-calculated methane hydrate lattice constants as a function of temperature at 1 bar using the TIP4P/Ice (red up triangles) and TIP4P/2005 (blue down triangles) force fields for water. Second order polynomial fits of the MD data are also shown as solid lines for the case of TIP4P/Ice (red line) and TIP4P/2005 (blue line) force fields for water. Experimental data for the methane hydrate lattice constants by Ogienko et al. (solid black line) [16] and Shpakov et al. (dashed black line) [13], as well as data for the deuterated methane hydrate by Gutt et al. (dotted black line) [14] are also shown. Finally, MD data by Jiang et al. [29] using the AMOEBA and COS polarisable force fields are shown by the black squares and diamonds, respectively, and MD data by Jiang and Jordan [30] using SPC/E are shown by the black stars. (For interpretation of the references to colour in this figure legend, the reader is referred to the web version of the article).

1000 bar. The MD results are shown in Figure 5. There is a systematic difference between the predictions of the two force fields for a given temperature and pressure. We observe that the linear fits provide an excellent description of the MD simulations.

These three temperatures are the ones considered in the recent MC study of Papadimitriou et al. [40] where the methane storage capacities of different structures of hydrates were calculated. Traditionally, such MC studies [67,68] assume a constant value for the lattice constant, without considering its variation as a function of pressure. This assumption, usually, has a relatively small effect on the calculated storage capacities. For example, a 0.6% change in the lattice constant can result in less than 3% change in the storage capacity of structure sII H_2 hydrate [67]. We observe in Figure 5 that for a particular temperature the percentage deviation between the maximum and minimum values that were calculated for the lattice constants is up to 0.20% (200 K), 0.24% (250 K) and 0.28% (300 K) for the case of TIP4P/Ice. The corresponding values for TIP4P/2005 are slightly higher: 0.26% (200 K), 0.29% (250 K) and 0.33% (300 K), respectively. On the

other hand, as Hester et al. [20] pointed out a 0.5% change in the lattice constant can result in more than 15% change in the predicted hydrate equilibrium pressure (at pressures higher than 100 MPa for methane).

For the case of carbon dioxide, two different temperature and pressure ranges are considered. The first includes temperatures equal to 200, 240 and 280 K and pressures up to 300 bar (shown in Figure 6), while the second includes temperatures equal to 283.15 and 293.15 K and pressures up to 5000 bar (shown in Figure 7). The motivation behind this particular distinction is the fact that carbon dioxide has an upper quadruple point, Q_2, at 283.1 K and 45.02 bar (Unruh and Katz [69]), where four phases are at equilibrium ($H–L_w–V–L_{CO2}$). For temperatures and pressures that are above those corresponding to Q_2 the phases at equilibrium are $H–L_w–L_{CO2}$. This was also the pressure and temperature range examined in the recent MD study of Costandy et al. [36]. Here again, at any temperature and pressure examined the lattice constant predicted by TIP4P/Ice is higher than the lattice constant predicted by TIP4P/2005. We observe in Figure 6 that for a particular
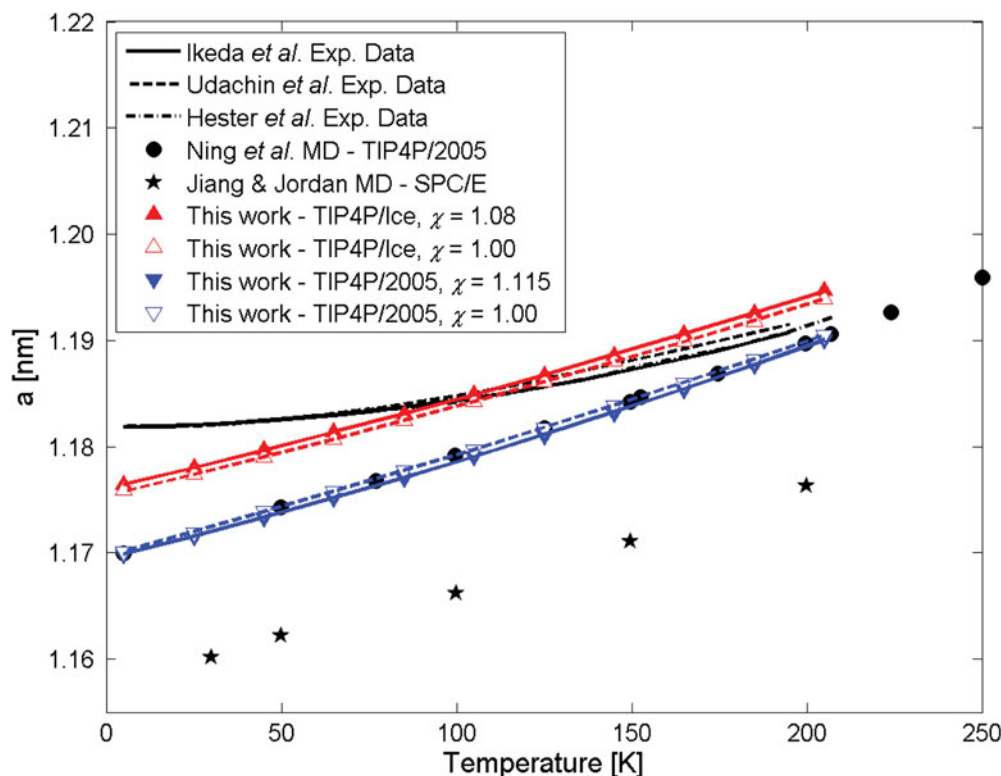
Figure 4. MD-calculated carbon dioxide hydrate lattice constants as a function of temperature at 1 bar using the TIP4P/Ice (red up triangles) and TIP4P/2005 (blue down triangles) force fields for water for the cases where the cross-interactions are calculated using the LB combining rules (open symbols) and using the modification parameters χ (solid symbols) for the two force fields. Second order polynomial fits of the MD data are also shown for the case of TIP4P/Ice (red lines) and TIP4P/2005 (blue lines) force fields for water. The black circles denote the MD results by Ning *et al.* [43] using the TIP4P/2005 and TraPPE for water and carbon dioxide, respectively, while the black stars denote the MD results by Jiang and Jordan using the SPC/E and the ZD for water and carbon dioxide, respectively. Experimental data by Ikeda *et al.* (solid black line) [17], Udachin *et al.* (dashed black line) [19] and Hester *et al.* (dashed-dotted black line) [20] are also shown. (For interpretation of the references to colour in this figure legend, the reader is referred to the web version of the article).

temperature, the percentage deviation between the maximum and minimum values that were calculated for the lattice constants is up to 0.10% for both TIP4P/Ice and TIP4P/2005 water models (for the pressure range 30–300 bar). On the other hand, in Figure 7 the percentage deviation between the maximum and minimum values that were calculated for the lattice constants is up to 1.56% and 1.78% for TIP4P/Ice and TIP4P/2005 water models, respectively (for the pressure range 200–5000 bar). Essentially, in both cases considered (i.e. Figures 6 and 7) an increase of the deviation that is equal to 0.037% for every 100 bar increase in pressure was obtained.

3.4. Isothermal compressibility

The isothermal compressibility, κ_T, of hydrates is an important parameter that is encountered during the interpretation of seismic data obtained during the geophysical surveys that are performed in order to identify natural hydrate deposits within off-shore oceanic sediments or on-shore permafrost settings [70]. In particular, the bulk modulus [71] of hydrate, which is defined as

the inverse compressibility (i.e. $B_T = \frac{1}{\kappa_T}$), is an essential input parameter for the analysis of the obtained logging data, since solid hydrates contribute as well to the frame bulk modulus (i.e. the porous matrix saturated with fluids and crystal hydrate) [72,73].

The isothermal compressibility [43] of hydrates can be calculated using the following equation for all the temperatures of interest:

$$\kappa_T = -\frac{1}{V}\left(\frac{\partial V}{\partial P}\right)_T \tag{3}$$

where V is the volume of the hydrate unit cell. Earlier MD studies [43] have used the volume of the unit cell, as calculated by the MD simulations, in order to fit the calculated values to second order polynomials as follows:

$$V(P) = m_{P0} + m_{P1} \cdot (P/bar) + m_{P2} \cdot (P/\text{bar})^2,$$
$$\text{for } T \text{ constant} \tag{4}$$

where P is the pressure and, m_{P0}, m_{P1} and m_{P2} are guest-specific constants. The particular constants that were
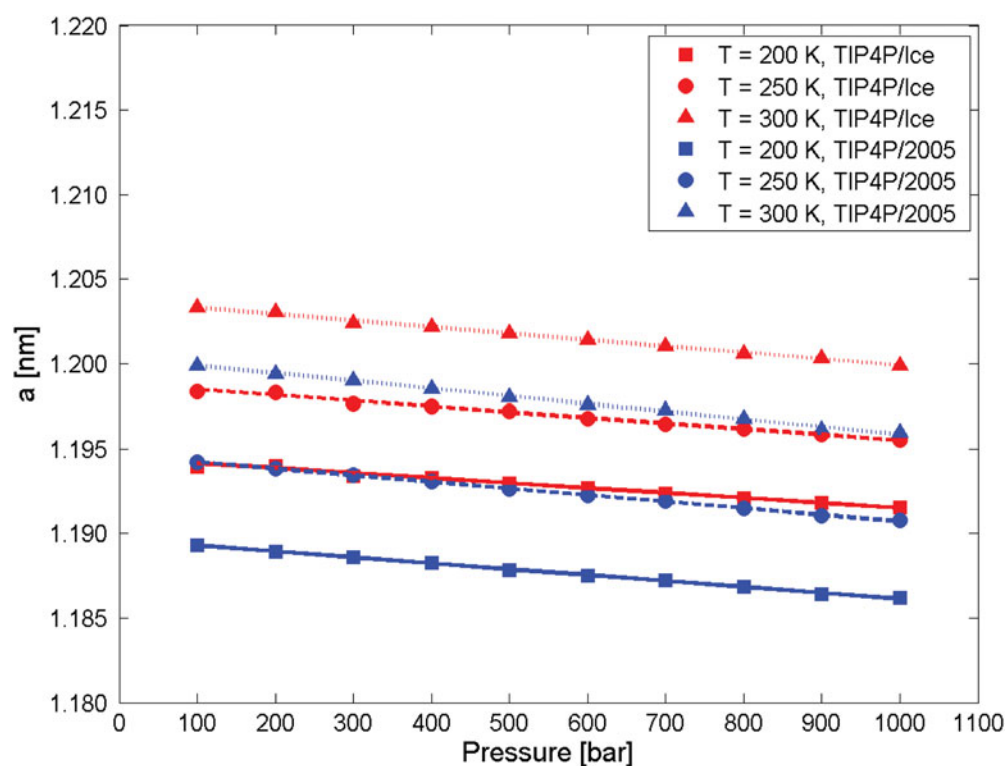
Figure 5. MD results for methane hydrate lattice constant as a function of pressure at 200 (squares), 250 (circles) and 300 K (triangles) using the TIP4P/Ice (red) and TIP4P/2005 (blue) force fields for water. Linear fits of the MD data are also shown using solid, dashed and dotted lines for 200, 250 and 300 K, respectively. (For interpretation of the references to colour in this figure legend, the reader is referred to the web version of the article).

Figure 6. MD results for carbon dioxide hydrate lattice constant as a function of pressure at 200 (squares), 240 (circles) and 280 K (triangles) temperatures using the TIP4P/Ice (red) and TIP4P/2005 (blue) force fields for water. Linear fits of the MD data are also shown using solid, dashed and dotted lines for 200, 240 and 280 K, respectively. (For interpretation of the references to colour in this figure legend, the reader is referred to the web version of the article).
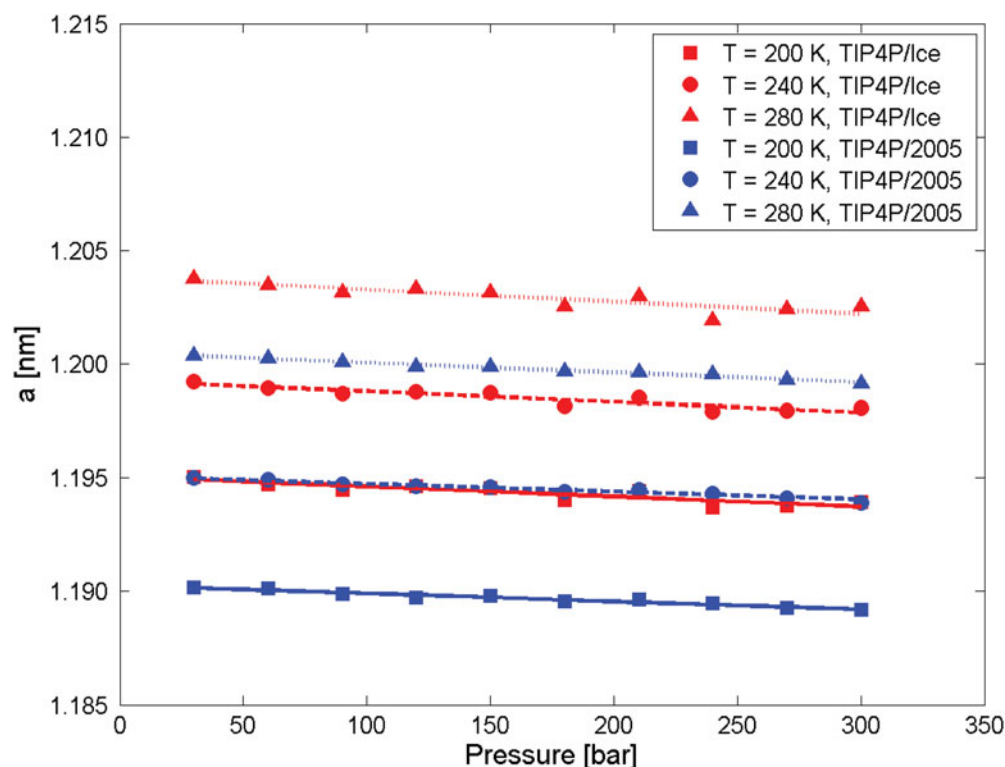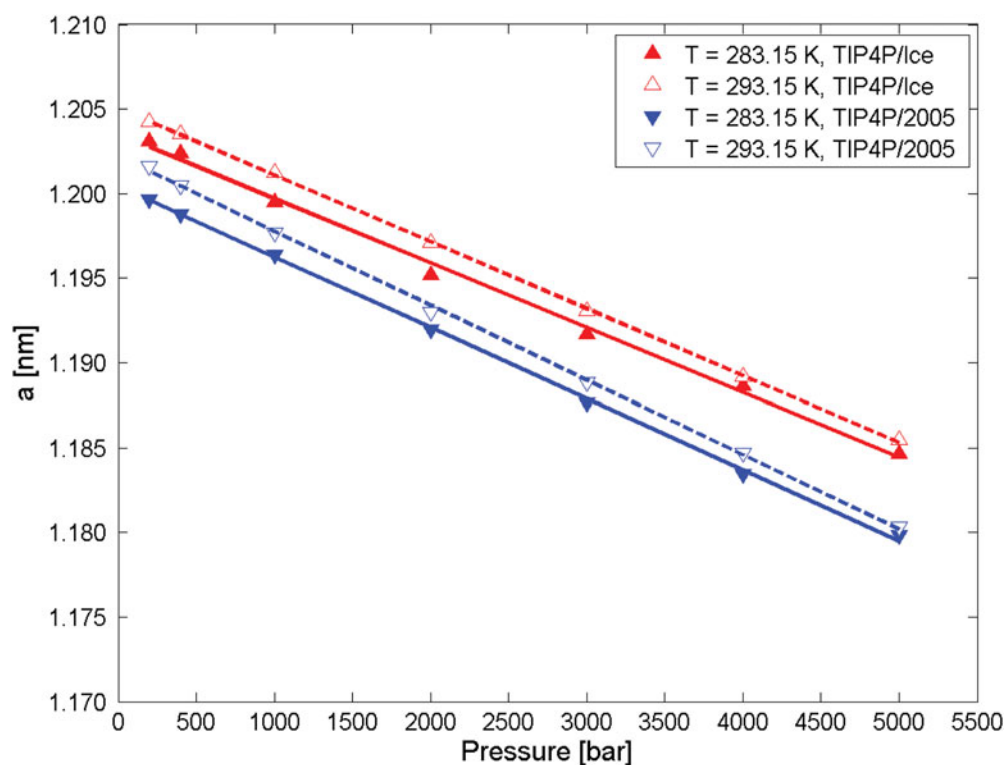
Figure 7. MD results for carbon dioxide hydrate lattice constant as a function of pressure at 283.15 (solid symbols) and 293.15 K (open symbols) using the TIP4P/Ice (red) and TIP4P/2005 (blue) force fields for water. Linear fits of the MD data are also shown. (For interpretation of the references to colour in this figure legend, the reader is referred to the web version of the article).
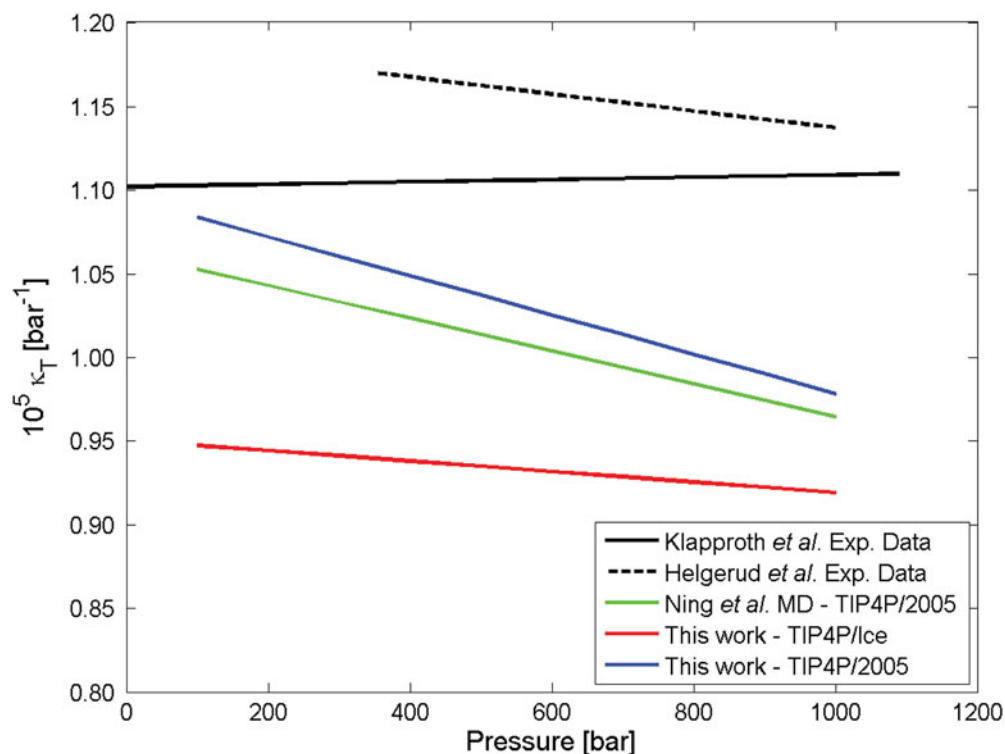
Figure 8. Methane hydrate isothermal compressibility as a function of pressure at 271.15 K using the TIP4P/Ice (red line) and TIP4P/2005 (blue line) force fields for water. The solid green line shows the simulations by Ning *et al.* [43] using TIP4P/2005. The solid black line depicts the calculated isothermal compressibility from the lattice constant data provided by Klapproth *et al.* [12], while the dashed black line shows the compressibility calculations that are based to the correlation of experimental data for bulk modulus reported by Helgerud *et al.* [74]. (For interpretation of the references to colour in this figure legend, the reader is referred to the web version of the article).

Figure 9. Methane hydrate isothermal compressibility as a function of pressure at 200 (solid lines), 250 (dashed lines) and 300 K (dotted lines) temperatures using the TIP4P/Ice (red) and TIP4P/2005 (blue) force fields for water. (For interpretation of the references to colour in this figure legend, the reader is referred to the web version of the article).

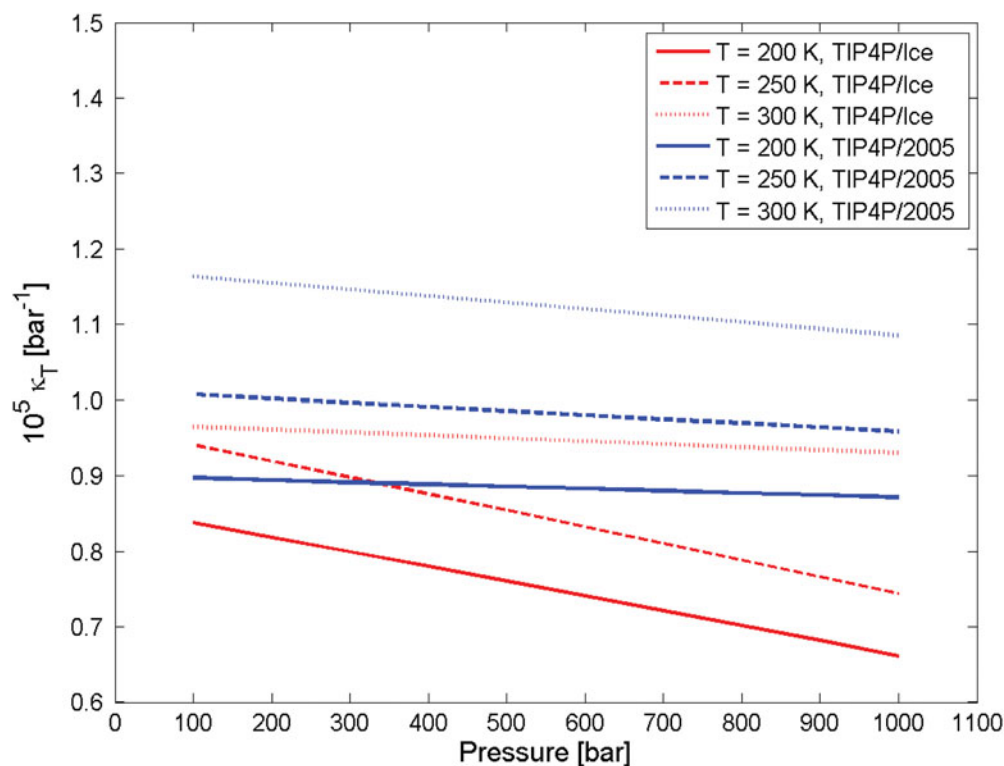calculated by the current study are given in Tables SI-5 and SI-6 of the Supplemental Information for methane and carbon dioxide hydrates, respectively. Therefore, the isothermal compressibility can be calculated by the differentiation of Equation (4). Such an approach was followed in the current study as well.

Figure 8 shows the dependence of the pure methane hydrate isothermal compressibility on pressure at 271.15 K using the TIP4P/Ice and TIP4P/2005 force fields for water and the calculated isothermal compressibilities from the lattice constant data provided by Klapproth *et al*. [12]. To this purpose, we used a second degree polynomial to describe the optimum-fit line of the reported experimental data for the lattice constants. This approach resulted in an isothermal compressibility that is essentially independent of pressure. Note, however, that the experimental data for the lattice constant exhibit a scatter and the resulting slope of the compressibility is sensitive to the values of the lattice constants. Shown also in Figure 8 are the values for the pure methane hydrate isothermal compressibility that can be calculated using the experimental correlation for the bulk modulus that was reported by Helgerud *et al*. [74]. The authors performed an extensive series of experiments in the temperature range (−20 to 15 °C) and pressure range

(30.5–97.7) MPa and correlated their experimental measurements for the bulk modulus, B_T, using a functional of the type, $B_T(T, P) = aT + bP + c$, where a, b, c are constants [74].

In general, we observe that the simulations using the TIP4P/2005 water model resulted in obtaining compressibilities that are closer to the experimental results by Klapproth *et al*. [12] and Helgerud *et al*. [74]. On the other hand, simulations using the TIP4P/Ice water model produce a slope for the compressibility (i.e. when plotting k_T vs. P) that is in better agreement with the experimental data. Note that the difference observed with the data of Klapproth *et al*. [12] is due to: (1) the scatter of the experimental data for lattice constants and (2) the increased sensitivity of the resulting slope of the compressibility on the scatter of the experimental data. In addition, we observe very good agreement between the current results and those reported earlier by Ning *et al*. [43]. Both MD simulation studies ([43], and this work) exhibit a trend that is in good agreement with the experimental data reported by Helgerud *et al*. [74].

Figure 9 shows the dependence of the pure methane hydrate isothermal compressibility on pressure at temperatures equal to 200, 250 and 300 K using the TIP4P/Ice and TIP4P/2005 force fields for water. Such temperature
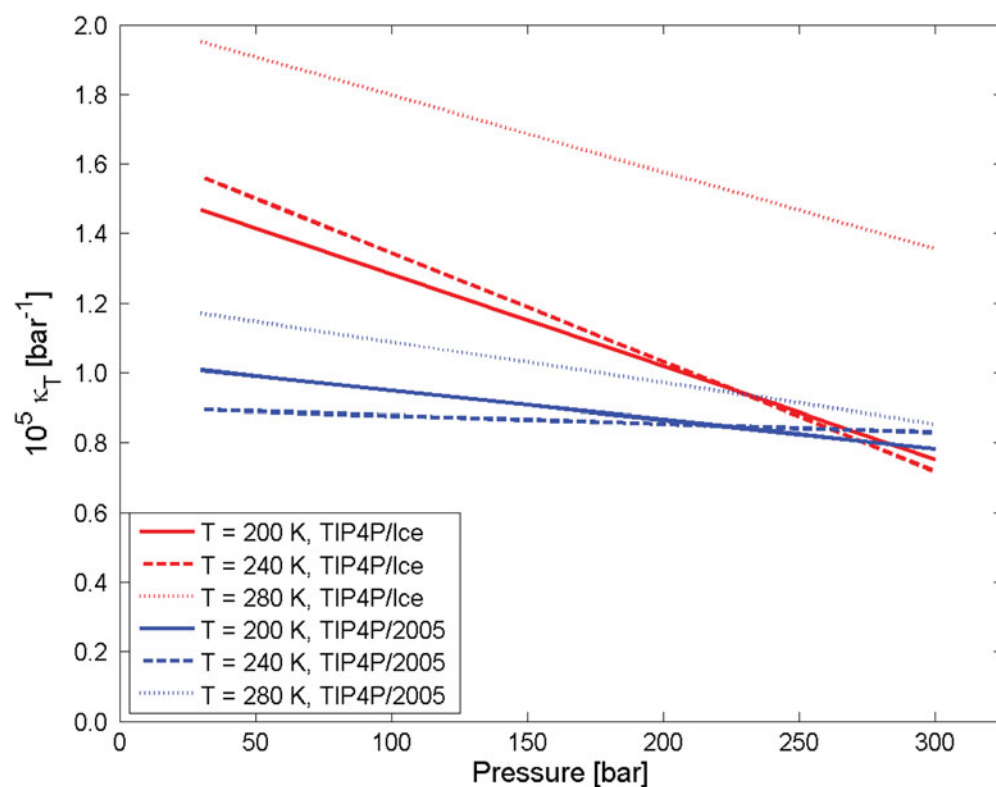
Figure 10. Carbon dioxide hydrate isothermal compressibility as a function of pressure at 200 (solid lines), 240 (dashed lines) and 280 K (dotted lines) temperatures using the TIP4P/Ice (red) and TIP4P/2005 (blue) force fields for water. (For interpretation of the references to colour in this figure legend, the reader is referred to the web version of the article).
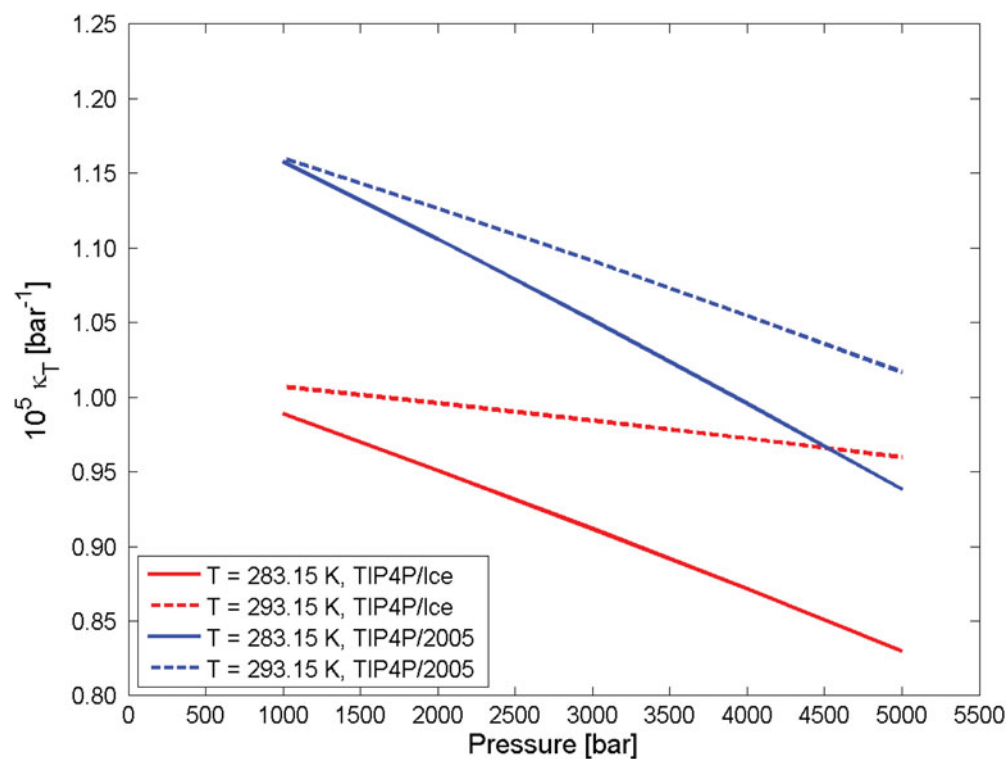
Figure 11. Carbon dioxide hydrate isothermal compressibility as a function of pressure at 283.15 (solid lines) and 293.15 K (dashed lines) temperatures using the TIP4P/Ice (red) and TIP4P/2005 (blue) force fields for water. (For interpretation of the references to colour in this figure legend, the reader is referred to the web version of the article).
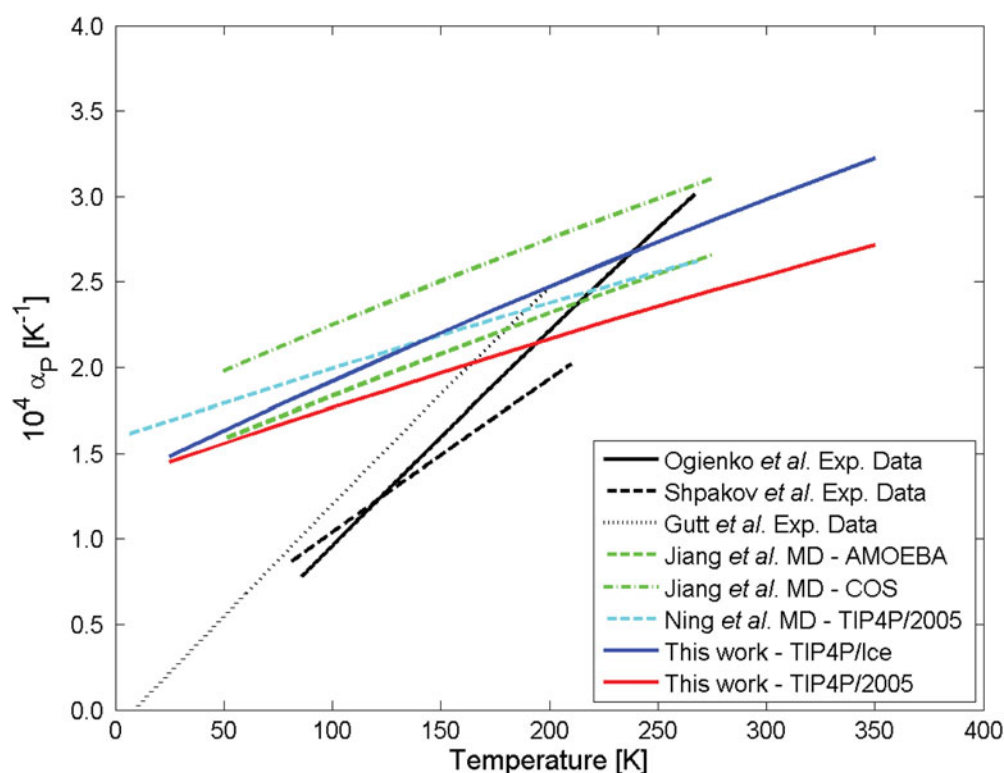
Figure 12. Methane hydrate thermal expansion coefficient as a function of temperature at 1 bar using the TIP4P/Ice (blue) and TIP4P/2005 (red) force fields for water. (For interpretation of the references to colour in this figure legend, the reader is referred to the web version of the article).
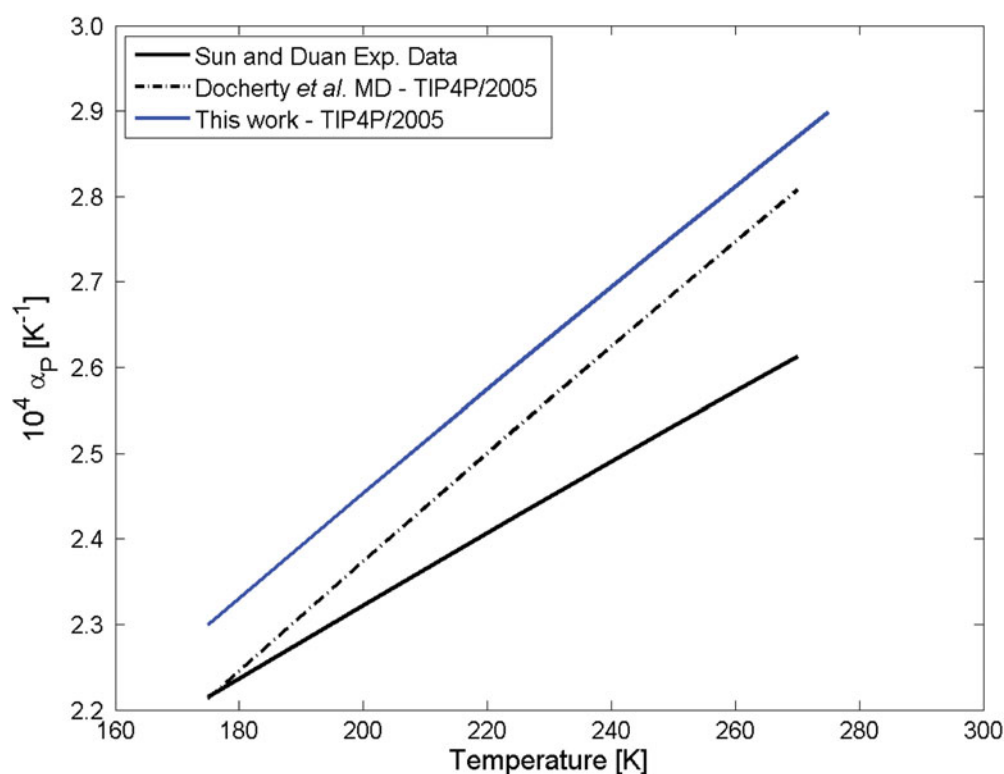
Figure 13. Methane hydrate thermal expansion coefficient as a function of temperature at 30 bar using the TIP4P/2005 force field for water. Comparison between the current simulations (blue solid line) with the simulations by Docherty *et al.* [28], and the experimental data by Sun and Duan [61]. (For interpretation of the references to colour in this figure legend, the reader is referred to the web version of the article).

Figure 14. Carbon dioxide hydrate thermal expansion coefficient as a function of temperature at 1 bar using the TIP4P/Ice (red) and TIP4P/2005 (blue) force fields for water for the cases where the cross-interactions are calculated using the LB combining rules (dashed lines) and using the modification parameters χ (solid lines) for the two force fields. (For interpretation of the references to colour in this figure legend, the reader is referred to the web version of the article).

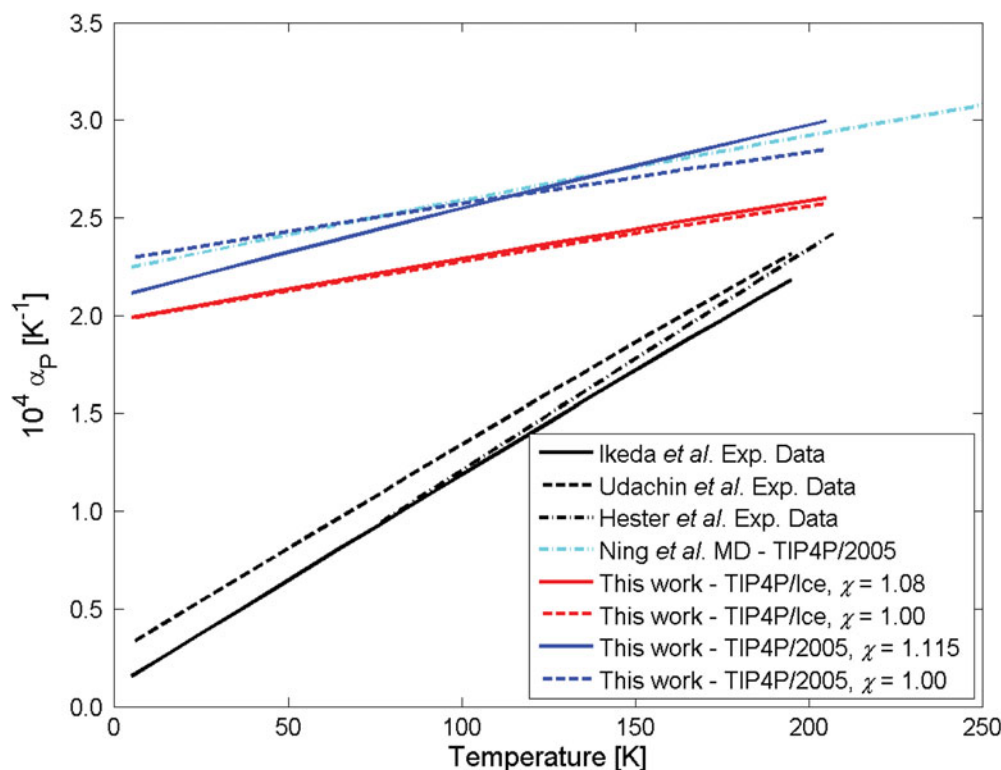and pressure conditions have been of interest to recent gas storage studies [40] with MC simulations. The following general observations can be made:

- For a fixed temperature the compressibility decreases as the pressure increases.
- For a fixed pressure the compressibility increases as the temperature increases.
- The use of TIP4P/2005 water model results in higher compressibility for the same P, T conditions.

Figure 10 shows the dependence of the carbon dioxide hydrate isothermal compressibility on pressure (up to 300 bar) at three different temperatures (200, 240 and 280 K) using the TIP4P/Ice and TIP4P/2005 water force fields, while Figure 11 shows the dependence of the carbon dioxide hydrate isothermal compressibility on pressure (up to 5000 bar) at two different temperatures (283.15 and 293.15 K) using the same water force fields. P, T conditions of Figure 10 are below the upper quadruple point, while conditions of Figure 11 correspond to above the upper quadruple point. Such conditions were the focus of recent MD studies [35,36] that examined the three-phase coexistence of the CO_2–H_2O system. The general observations that were reported earlier for methane hydrate hold for the case of carbon dioxide hydrate as well.

3.5. Isobaric thermal expansion coefficient

The isobaric thermal expansion coefficient, α_P, can be calculated using the following equation for all pressures of interest:

$$\alpha_P = \frac{1}{V}\left(\frac{\partial V}{\partial T}\right)_P \tag{5}$$

Similarly to the case of isothermal compressibility, the volume of the unit cell has been fitted during earlier studies [43] with second order polynomials as follows:

$$
\begin{aligned}
V(T) = m_{T0} &+ m_{T1} \cdot (T/K) \\
&+ m_{T2} \cdot (T/K)^2, \text{ for } P \text{ constant}
\end{aligned}
\tag{6}
$$

where T is in K and m_{T0}, m_{T1} and m_{T2} are constants. The particular constants that were calculated by the current study are given in Tables SI-7 and SI-8 of the Supplemental Information for methane and carbon dioxide hydrates, respectively.

Alternatively, the thermal expansion coefficient, α_P, could be calculated using the following equation for all pressures of interest with appropriate differentiation of

Equation (2):

$$\alpha_P = \frac{3}{a}\left(\frac{\partial a}{\partial T}\right)_P \qquad (7)$$

For Equation (7), we have also assumed that the volume of the unit cell and the lattice constants are related through: $V = a^3$.

Figure 12 shows the dependence of the pure methane hydrate thermal expansion coefficient on temperature at 1 bar using the TIP4P/Ice and TIP4P/2005 force fields for water, while Figure 13 shows the dependence of the methane hydrate thermal expansion coefficient on temperature at 30 bar using the TIP4P/2005 force field for water. We observe in Figure 13 that our MD simulations result in a similar slope, as the earlier simulation study of Docherty et al. [28]. On the other hand, however, our MD simulations are in worse agreement with experiments, compared to the earlier studies [28].

Figure 14 shows the dependence of the pure carbon dioxide hydrate thermal expansion coefficient on temperature at 1 bar using both water force fields for the cases where the cross-interactions are calculated using the LB combining rules with or without a modification parameters χ. It is evident from Figure 12 through Figure 14 that the particular water models that were examined are not capable of capturing the correct behaviour of the isobaric thermal expansion coefficient at low temperatures. In particular, the calculated thermal expansion coefficients do not approach the value of zero as the temperature approaches 0 K. This behaviour is a direct consequence of the fact that the models cannot describe accurately the true behaviour of the lattice constants that approach asymptotically a constant value at low T's, as discussed earlier in Section 3.2 (see also Figures 3 and 4). This is an inherent deficiency of the particular water models. A detailed discussion on the issue, and a simple methodology to rectify the problem, has been presented recently by Costandy et al. [66].

4. Conclusions

Pure methane and carbon dioxide hydrates were simulated using MD simulations. Simple polynomials were used in order to fit the obtained lattice constants. Subsequently, derivative structural properties were calculated by differentiation of the obtained polynomials. In particular, the isothermal compressibilities and the isobaric thermal expansion coefficients were calculated and compared to reported experimentally measured and numerically calculated values. The calculated isothermal compressibilities exhibit behaviour that is similar to previously reported experimental and computational

studies. On the other hand, the calculated isobaric thermal expansion coefficients are in agreement with other computational studies, while failing to capture the experimental behaviour at low temperatures.

ORCID

Joseph Costandy http://orcid.org/0000-0002-7275-4640
Vasileios K. Michalis http://orcid.org/0000-0003-3070-3949
Ioannis N. Tsimpanogiannis http://orcid.org/0000-0002-3466-1873
Athanassios K. Stubos http://orcid.org/0000-0001-8449-1932
Ioannis G. Economou http://orcid.org/0000-0002-2409-6831

References

[1] E.D. Sloan, Nature **426**, 353 (2003).
[2] E.D. Sloan and C.A. Koh, *Clathrate Hydrates of Natural Gases*, 3rd ed. (CRC Press, Boca Raton, FL, 2008).
[3] A.A. Khokhar, J.S. Gudmundsson, and E.D. Sloan, Fluid Phase Equilib. **150–151**, 383 (1998).
[4] S. Thomas and R.A. Dawe, Energy **28**, 1461 (2003).
[5] W.L. Mao and H.K. Mao, Proc. Natl. Acad. Sci. USA **101**, 708 (2004).
[6] V.V. Struzhkin, B. Militzer, W.L. Mao, H.K. Mao, and R.J. Hemley, Chem. Rev. **107**, 4133 (2007).
[7] H.P. Veluswamy, R. Kumar, and P. Linga, Appl. Energy **122**, 112 (2014).
[8] Y. Park, D.Y. Kim, J.W. Lee, D.G. Huh, K.P. Park, J. Lee, and H. Lee, Proc. Natl. Acad. Sci. USA **103**, 12690 (2006).
[9] X.-X. Zhang, H. Liu, C.-Y. Sun, P. Xiao, B. Liu, L.-Y. Yang, C.-H. Zhan, X.-Q. Wang, N. Li, and G.-J. Chen, Sep. Purif. Technol. **130**, 132 (2014).
[10] C.-G. Xu and X.-S. Li, RSC Advances **4**, 18301 (2014).
[11] P. Babu, P. Linga, R. Kumar, and P. Englezos, Energy **85**, 261 (2015).
[12] A. Klapproth, E. Goreshnik, D. Staykova, H. Klein, and W.F. Kuhs, Can. J. Phys. **81**, 503 (2003).

[13] V.P. Shpakov, J.S. Tse, C.A. Tulk, B. Kvamme, and V.R. Belosludov, Chem. Phys. Lett. **282**, 107 (1998).

[14] C. Gutt, B. Asmussen, W. Press, M.R. Johnson, Y.P. Handa, and J.S. Tse, J. Chem. Phys. **113**, 4713 (2000).

[15] S. Takeya, M. Kida, H. Minami, H. Sakagami, A. Hachikubo, N. Takahashi, H. Shoji, V. Soloviev, K. Wallmann, N. Biebow, A. Obzhirov, A. Salomatin, and J. Poort, Chem. Eng. Sci. **61**, 2670 (2006).

[16] A.G. Ogienko, A.V. Kurnosov, A.Y. Manakov, E.G. Larionov, A.I. Ancharov, M.A. Sheromov, and A.N. Nesterov, J. Phys. Chem. B **110**, 2840 (2006).

[17] T. Ikeda, O. Yamamuro, T. Matsuo, K. Mori, S. Torii, T. Kamiyama, F. Izumi, S. Ikeda, and S. Mae, J. Phys. Chem. Solids **60**, 1527 (1999).

[18] T. Ikeda, S. Mae, O. Yamamuro, T. Matsuo, S. Ikeda, and R.M. Ibberson, J. Phys. Chem. A **104**, 10623 (2000).

[19] K.A. Udachin, C.I. Ratcliffe, and J.A. Ripmeester, J. Phys. Chem. B **105**, 4200 (2001).

[20] K.C. Hester, Z. Huo, A.L. Ballard, C.A. Koh, K.T. Miller, and E.D. Sloan, J. Phys. Chem. B **111**, 8830 (2007).

[21] S. Takeya, K.A Udachin, I.L. Mudrakovski, R. Susilo, and J.A. Ripmeester, J. Am. Chem. Soc. **132**, 524 (2010).

[22] D.W. Davidson, Y.P. Handa, C.I. Ratcliffe, J.A. Ripmeester, J.S. Tse, J.R. Dahn, F. Lee, and L.D. Calvert, Mol. Cryst. Liq. Cryst. **141**, 141 (1986).

[23] K. Murayama, S. Takeya, S. Alavi, and R. Ohmura, J. Phys. Chem. C **118**, 21323 (2014).

[24] S. Takeya, T. Uchida, Y. Kamata, J. Nagao, M. Kida, H. Minami, H. Sakagami, A. Hachikubo, N. Takahashi, and H. Shoji, Angew. Chem. **117**, 7088 (2005).

[25] N.J. English and J.M.D. MacElroy, Chem. Eng. Sci. **121**, 133 (2015).

[26] V.R. Belosludov, T.M. Inerbaev, O.S. Subbotin, R.V. Belosludov, J.I. Kudoh, and Y. Kawazoe, J. Supramol. Chem. **2**, 453 (2002).

[27] N.J. English and J.M.D. MacElroy, J. Comp. Chem. **24**, 1569 (2003).

[28] H. Docherty, A. Galindo, C. Vega, and E. Sanz, J. Chem. Phys. **125**, 074510 (2006).

[29] H. Jiang, K.D. Jordan, and C.E. Taylor, J. Phys. Chem. B **111**, 6486 (2007).

[30] H. Jiang and K.D. Jordan, J. Phys. Chem. C **114**, 5555 (2010).

[31] T. Makiya, T. Murakami, S. Takeya, A.K. Sum, S. Alavi, and R. Ohmura, Phys. Chem. Chem. Phys. **12**, 9927 (2010).

[32] M.M. Conde and C. Vega, J. Chem. Phys. **133**, 064507 (2010).

[33] M.M. Conde and C. Vega, J. Chem. Phys. **138**, 056101 (2013).

[34] V.K. Michalis, J. Costandy, I.N. Tsimpanogiannis, A.K. Stubos, and I.G. Economou, J. Chem. Phys. **142**, 044501 (2015).

[35] J.M. Miguez, M.M. Conde, J.-P. Torre, F.J. Blas, M.M. Pineiro, and C. Vega, J. Chem. Phys. **143**, 124505 (2015).

[36] J. Costandy, V.K. Michalis, I.N. Tsimpanogiannis, A.K. Stubos, and I.G. Economou, J. Chem. Phys. **143**, 094506 (2015).

[37] A.J.C. Ladd and L.V. Woodcock, Chem. Phys. Lett. **51**, 155 (1977).

[38] J.L.F. Abascal, E. Sanz, R.G. Fernandez, and C. Vega, J. Chem. Phys. **122**, 234511 (2005).

[39] J.L.F. Abascal and C. Vega, J. Chem. Phys. **123**, 234505 (2005).

[40] N.I. Papadimitriou, I.N. Tsimpanogiannis, I.G. Economou, and A.K. Stubos, J. Chem. Eng. Data **61**, 2886 (2016).

[41] H. Henley and A. Lucia, J. Nat. Gas Sci. Eng. **26**, 446 (2015).

[42] P.E. Brumby, D. Yuhara, D.T. Yu, A.K. Sum, and K. Yasuoka, Fluid Phase Equilib. **413**, 242 (2016).

[43] F.L. Ning, K. Glavatskiy, Z. Ji, S. Kjelstrup, and T.J.H. Vlught, Phys. Chem. Chem. Phys. **17**, 2869 (2015).

[44] J.S. Loveday and R.J. Nelmes, Phys. Chem. Chem. Phys. **10**, 937 (2008).

[45] H. Hirai, K. Komatsu, M. Honda, T. Kawamura, Y. Yamamoto, and T. Yagi, J. Chem. Phys. **133**, 124511 (2010).

[46] R.K. McMullan and G.A. Jeffrey, J. Chem. Phys. **42**, 2725 (1965).

[47] F. Takeuchi, M. Hiratsuka, R. Ohmura, S. Alavi, A.K. Sum, and K. Yasuoka, J. Chem. Phys. **138**, 124504 (2013).

[48] J.D. Bernal and R.H. Fowler, J. Chem. Phys. **1**, 515 (1933).

[49] W.L. Jorgensen, J. Chandrasekhar, J.D. Madura, R.W. Impey, and M.L. Klein, J. Phys. Chem. **79**, 926 (1983).

[50] W.L. Jorgensen, J.D. Madura, and C.J. Swenson, J. Am. Chem. Soc. **106**, 6638 (1984).

[51] J.J. Potoff and J.I. Siepmann, AIChE J. **47**, 1676 (2001).

[52] M.P. Allen and D.J. Tildesley, *Computer Simulation of Liquids* (Oxford Science Publications, New York, 1989).

[53] D. van der Spoel, E. Lindahl, B. Hess, G. Groenhof, A.E. Mark, and H.J.C. Berendsen, J. Comput. Chem. **26**, 1701 (2005).

[54] B. Hess, C. Kutzner, D. van der Spoel, and E. Lindahl, J. Chem. Theory Comput. **4**, 435 (2008).

[55] S. Pronk, S. Pall, P. Larsson, P. Bjelkmar, R. Apostolov, M.R. Shirts, J.C. Smith, P.M. Kasson, D. van der Spoel, B. Hess, and E. Lindahl, Bioinformatics **29**, 845 (2013).

[56] H.J.C. Berendsen, J.P.M. Postma, W.F. van Gunsteren, A. DiNola, and J.R. Haak, J. Chem. Phys. **81**, 3684 (1984).

[57] U. Essmann, L. Perera, M.L. Berkowitz, T. Darden, H. Lee, and L.G. Pedersen, J. Chem. Phys. **103**, 8577 (1995).

[58] S.T. John, M.L. Klein, and I.R. McDonald, J. Chem. Phys. **81**, 6146 (1984).

[59] P. Ren and J.W. Ponder, J. Phys. Chem. B **107**, 5933 (2003).

[60] H. Yu and W.F. van Gunsteren, J. Chem. Phys. **121**, 9549 (2004).

[61] R. Sun and Z. Duan, Geochim. Cosmochim. Acta **69**, 4411 (2005).

[62] Z.G. Zhang and Z.H. Duan, J. Chem. Phys. **122**, 214507 (2005).

[63] Z.H. Duan and Z.G. Zhang, Geochim. Cosmochim. Acta **70**, 2311 (2006).

[64] C. McBride, C. Vega, E.G. Noya, R. Ramirez, and L.M. Sese, J. Chem. Phys. **131**, 024506 (2009).

[65] M.M. Conde, C. Vega, C. McBride, E.G. Noya, R. Ramirez, and L.M. Sese, J. Chem. Phys. **132**, 114503 (2010).

[66] J. Costandy, V.K. Michalis, I.N. Tsimpanogiannis, A.K. Stubos, and I.G. Economou, J. Chem. Phys. **144**, 124512 (2016).

[67] N.I. Papadimitriou, I.N. Tsimpanogiannis, A.Th. Papaioannou, and A.K. Stubos, J. Phys. Chem. C **112**, 10294 (2008).

[68] N.I. Papadimitriou, I.N. Tsimpanogiannis, I.G. Economou, and A.K. Stubos, Mol. Phys. **112**, 2258 (2014).

[69] C.H. Unruh and D.L. Katz, Trans. AIME **186**, 83 (1949).

[70] G. Guerin, D. Goldberg, and A. Meltser, J. Geophys. Res. **104B**, 17781 (1999).

[71] F. Ning, Y. Yu, S. Kjelstrup, T.J.H. Vlugt, and K. Glavatskiy, Energy Environ. Sci. **5**, 6779 (2012).

[72] M.B. Helgerud, J. Dvorkin, A. Nur, A. Sakai, and T. Collett, Geophys. Res. Lett. **26**, 2021 (1999).

[73] D. Gei and J.M. Carcione, Geophys. Prospect. **51**, 141 (2003).

[74] M.B. Helgerud, W.F. Waite, S.H. Kirby, and A. Nur, J. Geophys. Res. **114B**, 02212 (2009); Correction, J. Geophys. Res. **114B**, 04299 (2009).

Molecular Dynamics Study of Pure Methane and Carbon Dioxide Hydrates. Lattice Constants and Derivative Properties

Supplemental Information

Joseph Costandy[1,¥], Vasileios K. Michalis[1], Ioannis N. Tsimpanogiannis[1,2,*], Athanassios K. Stubos[2], and Ioannis G. Economou[1,*]

[1]*Chemical Engineering Program, Texas A&M University at Qatar, PO Box 23847, Doha, Qatar*

[2]*Environmental Research Laboratory, National Center for Scientific Research NCSR "Demokritos", 15310 Aghia Paraskevi Attikis, Greece*

[¥] *Current address: Artie McFerrin Department of Chemical Engineering, Texas A&M University, College Station, TX 77840, USA.*

Corresponding author at:

i.tsimpanogiannis@qatar.tamu.edu (Ioannis N. Tsimpanogiannis)

Table SI–1. Fitting parameters for the linear fits of the lattice constant of the methane hydrate as a function of pressure data at different temperatures using both the TIP4P/Ice and TIP4P/2005 force fields ($n_{P2} = 0$).

Guest	H$_2$O model	χ	T (K)	n_{P0}	n_{P1} (x10^{-6})	R^2
CH$_4$	TIP4P/2005	1.00	200	1.18963	-3.50176	0.99781
CH$_4$	TIP4P/2005	1.00	250	1.19461	-3.90764	0.99919
CH$_4$	TIP4P/2005	1.00	271.15	1.19693	-4.08208	0.99828
CH$_4$	TIP4P/2005	1.00	300	1.20034	-4.49008	0.99750
CH$_4$	TIP4P/Ice	1.00	200	1.19445	-2.94492	0.98968
CH$_4$	TIP4P/Ice	1.00	250	1.19882	-3.32002	0.99323
CH$_4$	TIP4P/Ice	1.00	271.15	1.20088	-3.72823	0.99468
CH$_4$	TIP4P/Ice	1.00	300	1.20369	-3.79672	0.99625

Table SI–2. Fitting parameters for the linear fits of the lattice constant of the carbon dioxide hydrate as a function of pressure data at different temperatures using both the TIP4P/Ice and TIP4P/2005 force fields ($n_{P2} = 0$).

Guest	H$_2$O model	χ	T (K)	n_{P0}	n_{P1} (x10^{-6})	R^2
CO$_2$	TIP4P/2005	1.115	200	1.19026	-3.54289	0.95653
CO$_2$	TIP4P/2005	1.115	240	1.19509	-3.44583	0.94229
CO$_2$	TIP4P/2005	1.115	280	1.20048	-4.29550	0.98273
CO$_2$	TIP4P/2005	1.115	283.15	1.20045	-4.18650	0.99936
CO$_2$	TIP4P/2005	1.115	293.15	1.20219	-4.39968	0.99920
CO$_2$	TIP4P/Ice	1.08	200	1.19506	-4.42168	0.78947
CO$_2$	TIP4P/Ice	1.08	240	1.19924	-4.55842	0.83394
CO$_2$	TIP4P/Ice	1.08	280	1.20380	-5.29253	0.73601
CO$_2$	TIP4P/Ice	1.08	283.15	1.20352	-3.81344	0.99615
CO$_2$	TIP4P/Ice	1.08	293.15	1.20504	-3.94382	0.99977

Table SI–3. Fitting parameters for the second order polynomial fits of the lattice constant of the methane hydrate as a function of temperature data at different pressures using both the TIP4P/Ice and TIP4P/2005 force fields.

Guest	H$_2$O model	χ	P (bar)	n_{T0}	n_{T1} (x10^{-5})	n_{T2} (x10^{-8})	R^2
CH$_4$	TIP4P/2005	1.00	1	1.17455	5.38189	10.97836	0.99970
CH$_4$	TIP4P/2005	1.00	30	1.17483	4.78971	12.34286	0.99971
CH$_4$	TIP4P/Ice	1.00	1	1.18153	5.38243	8.04777	0.99989

Table SI–4. Fitting parameters for the second order polynomial fits of the lattice constant of the carbon dioxide hydrate as a function of temperature data at 1 bar using both the TIP4P/Ice and TIP4P/2005 force fields, and both the LB and modified combining rules.

Guest	H$_2$O model	χ	P (bar)	n_{T0}	n_{T1} (x10^{-5})	n_{T2} (x10^{-8})	R^2
CO$_2$	TIP4P/2005	1.115	1	1.16944	8.17946	9.11285	0.99997
CO$_2$	TIP4P/2005	1.00	1	1.16971	8.92358	5.88934	0.99993
CO$_2$	TIP4P/Ice	1.08	1	1.17603	7.76451	6.37351	0.99999
CO$_2$	TIP4P/Ice	1.00	1	1.17540	7.74751	6.13948	0.99992

Table SI–5. Optimum parameters for the second order polynomial fits of the unit cell volume of the methane hydrate as a function of pressure at different temperatures using both the TIP4P/Ice and TIP4P/2005 force fields.

Guest	H_2O model	χ	T (K)	m_{P0}	m_{P1} (x10^{-5})	m_{P2} (x10^{-10})	R^2
CH_4	TIP4P/2005	1.00	200	1.68366	-1.51518	3.02215	0.99784
CH_4	TIP4P/2005	1.00	250	1.70494	-1.72617	5.38005	0.99924
CH_4	TIP4P/2005	1.00	271.15	1.71508	-1.87798	10.88849	0.99846
CH_4	TIP4P/2005	1.00	300	1.72964	-2.02664	8.52530	0.99762
CH_4	TIP4P/Ice	1.00	200	1.70463	-1.46217	17.11485	0.99056
CH_4	TIP4P/Ice	1.00	250	1.72346	-1.65958	19.40441	0.99411
CH_4	TIP4P/Ice	1.00	271.15	1.73187	-1.64619	3.45942	0.99471
CH_4	TIP4P/Ice	1.00	300	1.74409	-1.69004	4.13161	0.99627

Table SI–6. Optimum parameters for the second order polynomial fits of the unit cell volume of the carbon dioxide hydrate as a function of pressure at different temperatures using both the TIP4P/Ice and TIP4P/2005 force fields.

Guest	H_2O model	χ	T (K)	m_{P0}	m_{P1} (x10^{-5})	m_{P2} (x10^{-10})	R^2
CO_2	TIP4P/2005	1.115	200	1.68641	-1.74015	70.65934	0.95767
CO_2	TIP4P/2005	1.115	240	1.70690	-1.53810	20.97980	0.94239
CO_2	TIP4P/2005	1.115	280	1.73009	-1.89854	13.06795	0.98276
CO_2	TIP4P/2005	1.115	283.15	1.73079	-1.94157	3.25777	0.99974
CO_2	TIP4P/2005	1.115	293.15	1.73856	-2.07354	4.00846	0.99971
CO_2	TIP4P/Ice	1.08	200	1.70721	-2.64102	226.91375	0.79607
CO_2	TIP4P/Ice	1.08	240	1.72527	-2.85618	270.24454	0.84307
CO_2	TIP4P/Ice	1.08	280	1.74554	-4.10214	546.82672	0.76023
CO_2	TIP4P/Ice	1.08	283.15	1.74529	-1.96851	6.74486	0.99855
CO_2	TIP4P/Ice	1.08	293.15	1.75028	-1.78158	1.82832	0.99987

Table SI–7. Optimum parameters for the second order polynomial fits of the unit cell volume of the methane hydrate as a function of temperature at different pressures using both the TIP4P/Ice and TIP4P/2005 force fields.

Guest	H$_2$O model	χ	P (bar)	m_{T0}	m_{T1} (x10^{-4})	m_{T2} (x10^{-7})	R^2
CH$_4$	TIP4P/2005	1.00	1	1.62063	2.16524	4.99667	0.99965
CH$_4$	TIP4P/2005	1.00	30	1.62242	1.86985	5.64513	0.99971
CH$_4$	TIP4P/Ice	1.00	1	1.64960	2.21375	3.70847	0.99987

Table SI–8. Optimum parameters for the second order polynomial fits of the unit cell volume of the carbon dioxide hydrate as a function of temperature at 1 bar using both the TIP4P/Ice and TIP4P/2005 force fields.

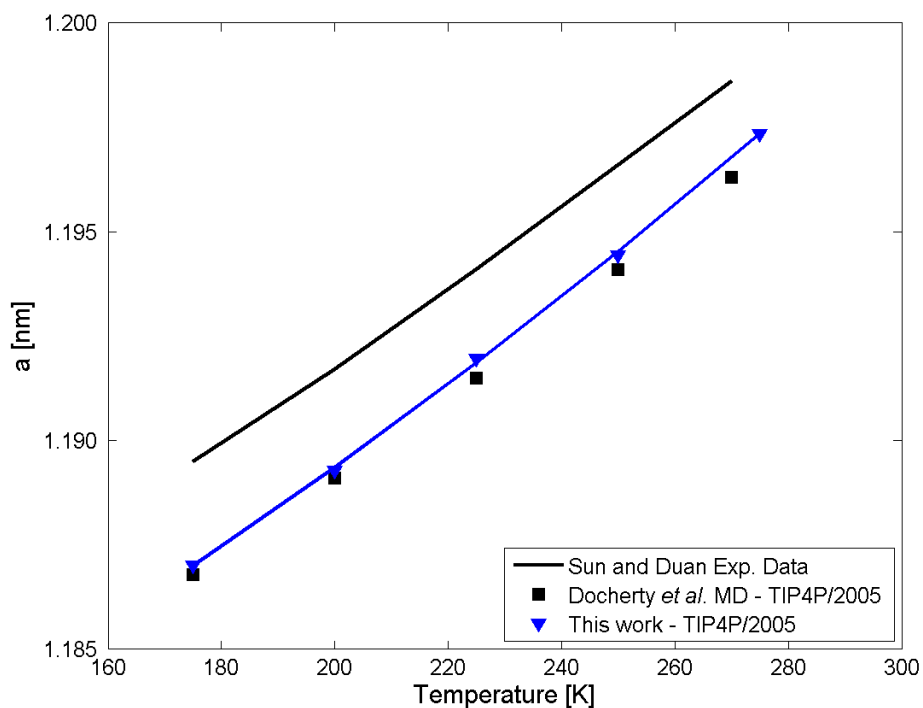| Guest	H$_2$O model	χ	P (bar)	m_{T0}	m_{T1} (x10^{-4})	m_{T2} (x10^{-7})	R^2
CO$_2$	TIP4P/2005	1.115	1	1.59936	3.33889	4.16696	0.99996
CO$_2$	TIP4P/2005	1.00	1	1.60044	3.65120	2.82917	0.99993
CO$_2$	TIP4P/Ice	1.08	1	1.62651	3.21073	2.98229	0.99999
CO$_2$	TIP4P/Ice	1.00	1	1.62391	3.20161	2.87188	0.99992

FIGURE SI–1. Dependence of the MD-calculated methane hydrate lattice constants on temperature at 30 bar using the TIP4P/2005 (blue down triangles) force field for water. A second order polynomial fit of the MD data is also shown (blue line). The solid black line denotes the experimental data for the methane hydrate lattice constants by Sun and Duan [61] at 30 bar. The black squares denote the MD data using the TIP4P/2005 force field by Docherty *et al.* [28].